NEURAL NETWORK-BASED EVALUATION OF SEISMIC RESPONSE OF STEEL MOMENT FRAMES

Z.H.F. Jafar and S. Gholizadeh[*, †]
Department of Civil Engineering, Urmia University, Urmia, Iran

ABSTRACT

The main objective of this study is to predict the maximum inter-story drift ratios of steel moment-resisting frame (MRF) structures at different seismic performance levels using feed-forward back-propagation (FFBP) neural network models. FFBP neural network models with varying numbers of hidden layer neurons (5, 10, 15, 20, and 50) were trained to predict the maximum inter-story drift ratios of 5- and 10-story steel MRF structures. The numerical simulations indicate that FFBP neural network models with ten hidden layer neurons better predict the inter-story drift ratios at seismic performance levels for both 5- and 10-story steel MRFs compared to other neural network models.

Keywords: seismic performance level; steel moment resisting frame; neural network; feed-forward back-propagation.

1. INTRODUCTION

Ensuring sufficient seismic resistance is crucial for any structure to remain available after an earthquake. Seismic design procedures employ performance-based design to achieve this goal [1]. These approaches involve using nonlinear structural analysis methods to evaluate the nonlinear inelastic response of structures. However, this is a challenging design procedure that requires a significant amount of computational effort. Structural engineers are concerned with designing cost-efficient, reliable structures that can withstand earthquakes. Performance-based design optimization techniques have been developed to address this issue, and numerous studies have been conducted in this field [2-7]. Metaheuristic algorithms are the best solution to the performance-based design optimization problem of structures. These algorithms are based on stochastic natural phenomena and do not require

---

[*]Corresponding author: Department of Civil Engineering, Urmia University, Urmia, P.O. box 165, Iran
[†]E-mail address: s.gholizadeh@urmia.ac.ir (S. Gholizadeh)

gradient computations, making computer implementation simple [8-12]. However, since metaheuristic algorithms are population-based search methods, the computational burden of performance-based design optimization using them is high because many nonlinear structural analyses must be performed. Neural networks are one of the best alternative solutions to reduce this burden.

In recent years, there has been an increasing interest in using artificial intelligence techniques, particularly neural networks, to simplify complex problems. Neural networks are computational models that imitate the structure and function of the human brain. They have shown success in numerous research areas of civil engineering [13-17] because of their capacity to learn from data and model complex nonlinear relationships. This paper uses neural network models to predict the nonlinear seismic response of steel moment-resisting frame (MRF) structures at different seismic performance levels.

Two design examples of 5-and 10-story SMFs are illustrated. Their maximum inter-story drift ratios are predicted using feed-forward back-propagation (FFBP) neural network models with different numbers of hidden layer neurons (5, 10, 15, 20, and 50), and the results are compared. The results indicate that the most accurate prediction is achieved by using ten hidden layer neurons.

2. SEISMIC RESPONSES OF STEEL MRF STRUCTURES

A seismic performance objective is a defined level of performance for a specific seismic hazard level. To establish a performance objective, one needs to determine a level of structural performance and the corresponding seismic hazard level. FEMA-356 [1] considers immediate occupancy (IO), life safety (LS), and collapse prevention (CP) performance levels. Each objective corresponds to a probability of exceedance in 50 years. IO, LS, and CP performance levels are assumed to correspond to a 50%, 10%, and 2% probability of exceedance in 50 years. Here, acceleration response spectra of the hazard levels are based on the Iranian seismic design code [18] for soil type III in a very high seismicity region, as shown in Fig. 1.
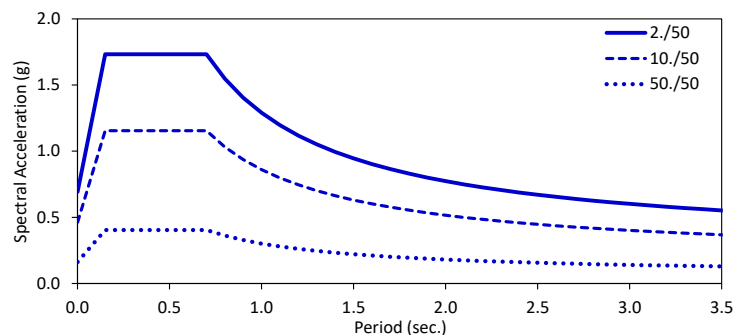

Figure 1. Acceleration response spectra

In seismic performance-based design, the structural response should be evaluated by performing nonlinear structural analysis. In this paper, a nonlinear static pushover analysis based on the displacement coefficient method [1] is performed using the OpenSees [19]

platform to evaluate the nonlinear structural response. Previous studies [20-23] have revealed that the seismic design of steel MRFs is typically dominated by maximum inter-story drift ratios, and other constraints, such as plastic rotations of beams and columns, are generally not active. Therefore, in this paper, only the maximum inter-story drift ratios at IO, LS, and CP performance levels are considered the seismic responses of the steel MRFs.

3. NEURAL NETWORKS

Neural networks are highly efficient tools for solving complex and time-consuming problems. They are popular because they can learn from external data and information gained from past experiences. Unlike traditional problem-solving methods that follow specific rules or use physics equations related to the issues they work on, neural networks use their knowledge from past experiences to adapt to new problems. Their learning is not limited to explicit and desired knowledge but also encompasses implicit information that the designer may not know beforehand [24]. This paper employs a feed-forward multi-layer perceptron trained by a back-propagation [24] technique. This neural network is called a feed-forward back-propagation (FFBP) model, shown in Fig. 2.
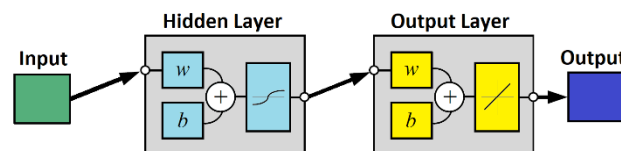

Figure 2. FFBP neural network model

The training algorithm of the FFBP model is a gradient descent optimization algorithm that adjusts the weights in the steepest descent direction according to the following equation:

$$W_{t+1} = W_t - \eta \nabla_t \tag{1}$$

where W_t, ∇_t, and η_t are the weight matrix, and the current gradient matrix learning rate, respectively, at iteration t.

the back-propagation technique uses the Levenberg-Marquardt (LM) [24] algorithm to approach second-order training speed without having to compute the Hessian matrix. In the LM algorithm, the updating of the weights is achieved as follows:

$$W_{t+1} = W_t - [J^T J + \alpha I]^{-1} J^T Er \tag{2}$$

where J is the Jacobian matrix, the first derivatives of the network errors to the weights); Er is a vector of network errors; α is a correction factor; and I is the identity matrix.

Regularization is a technique used to prevent overfitting in FFBP models. This is achieved by modifying the performance function of the model through the addition of a term. The added term consists of the mean of the sum of squares of the network weights. This is expressed as [24]:

$$mse_r = \gamma \left(\frac{1}{m} \sum_{k=1}^{m} (Er_k)^2 \right) + \frac{1-\gamma}{nw} \sum_{l=1}^{nw} \left(W_{t,l} \right)^2 \tag{3}$$

where γ and nw are the performance ratio and number of network weights, respectively; m is the size of Er_k.

4. METHODOLOGY

In this study, FFBP models predict the seismic response of planar steel MRFs encompassing 5- and 10-story frames. The topology and member grouping details of the structures are shown in Figs. 3 and 4, respectively.
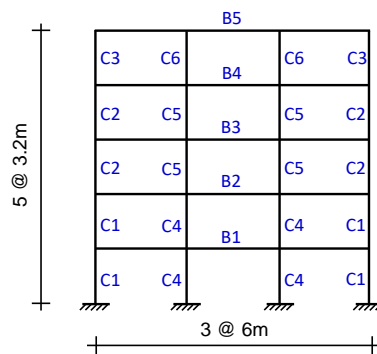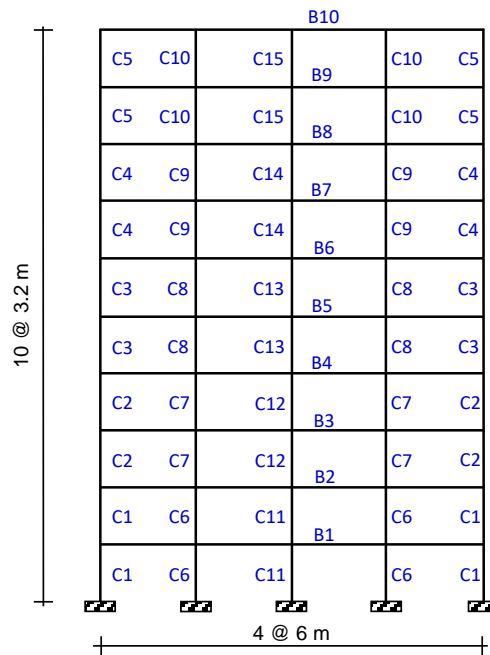

Figure 3. 5-story steel MRF

Figure 4. 10-story steel MRF

FFBP NN models are trained to predict maximum inter-story drift ratios of steel MRFs at seismic performance levels. For the 5- and 10-story steel SMFs, the input and output vectors of the NN models are as follows:

For 5-story steel SMF
$$X_5 = \{C1\ \ C2\ ...\ C6\ \ B1\ \ B2\ \ ...\ \ B5\}^T \tag{4}$$

For 10-story steel SMF
$$X_{10} = \{C1\ \ C2\ ...\ C15\ \ B1\ \ B2\ \ ...\ \ B10\}^T \tag{5}$$

For 5- and 10-story SMFs
$$Y = \{d_{IO}\ \ d_{LS}\ \ d_{CP}\}^T \tag{6}$$

where X_5 and X_{10} are the input vectors of the NN models for 5 and 10-story steel MRFs, respectively; Y is the output vector; and d_{IO}, d_{LS}, and d_{CP} are the maximum inter-story drift ratios of steel MRFs at IO, LS, and CP performance levels, respectively.

All the generated data samples for 5- and 10-story steel SMFs must satisfy geometric and strength constraints. Some checks should be considered the geometric constraints at all the framing joints. Fig. 5 shows a typical joint where a beam and two columns are connected, and based on these details, the following constraints must be met:
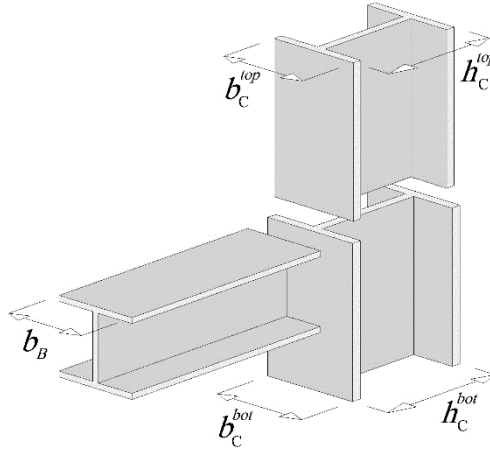

Figure 5. A typical framing joint

$$b_B \leq b_C^{bot} \tag{7}$$

$$b_C^{top} \leq b_C^{bot} \tag{8}$$

$$h_C^{top} \leq h_C^{bot} \tag{9}$$

As the strength constraints, each structural element should satisfy the following constraints for the non-seismic load combinations [25]:

For $\quad \dfrac{P_u}{\emptyset_c P_n} < 0,2 \quad \rightarrow \quad \dfrac{P_u}{2\emptyset_c P_n} + \dfrac{M_u}{\emptyset_b M_n} \leq 1,0 \tag{10}$

$$\text{For} \quad \frac{P_u}{\emptyset_c P_n} \geq 0{,}2 \quad \rightarrow \quad \frac{P_u}{\emptyset_c P_n} + \frac{8}{9}\frac{M_u}{\emptyset_b M_n} \leq 1{,}0 \tag{11}$$

where P_u is the required strength; P_n is the nominal axial strength; $\emptyset_c$ and $\emptyset_b$ are the resistance factors; M_u and M_n are the required and nominal flexural strengths, respectively.

If a structure passes the above checks, its seismic responses are evaluated by performing a nonlinear static pushover analysis based on the displacement coefficient method. Fig. 6 illustrates a detailed flowchart of dataset generation for training and testing the NN model.
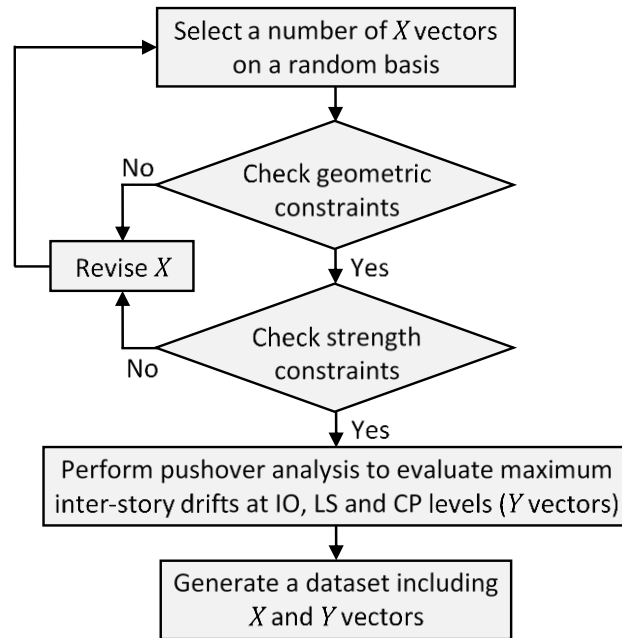

Figure 6. Dataset generation flowchart

The NN model's prediction accuracy evaluation metrics, including Mean Absolute Percentage Error (MAPE), Root Mean Square Error (RSME), and Coefficient of Determination (R-square or R^2) used in this study, are as follows:

$$\text{Mean Absolute Percentage Error} \quad MAPE = \frac{100}{ns}\sum_{i=1}^{ns}\left|\frac{t_i - y_i}{t_i}\right| \tag{12}$$

$$\text{Root Mean Square Error} \quad RMSE = \sqrt{\frac{1}{ns}\sum_{i=1}^{ns}(t_i - y_i)^2} \tag{13}$$

$$\text{Coefficient of Determination} \quad R^2 = 1 - \frac{\sum_{i=1}^{ns}(t_i - y_i)^2}{\sum_{i=1}^{ns}(t_i - \bar{t})^2} \tag{14}$$

where ns is the number of samples; t_i is the ith target maximum inter-story drift; y_i is ith predicted maximum inter-story drift; and $\bar{t}$ is the mean of target maximum inter-story drift.

In order to compare the efficiency of the trained FFBP models, average MAPE (AMAPE), average RMSE (ARMSE), and average R^2 (AR^2) of predicted inter-story drifts at IO, LS, and CP performance levels in both the training and testing phases are calculated as follows.

$$AMAPE_{d_{PL}} = \frac{\left(MAPE_{d_{PL}}\right)_{training} + \left(MAPE_{d_{PL}}\right)_{testing}}{2} \qquad PL = IO.LS.CP \qquad (15)$$

$$ARMSE_{d_{PL}} = \frac{\left(RMSE_{d_{PL}}\right)_{training} + \left(RMSE_{d_{PL}}\right)_{testing}}{2} \qquad PL = IO.LS.CP \qquad (16)$$

$$AR^2_{d_{PL}} = \frac{\left(R^2_{d_{PL}}\right)_{training} + \left(R^2_{d_{PL}}\right)_{testing}}{2} \qquad PL = IO.LS.CP \qquad (17)$$

This paper considers five FFBP NN models with 5, 10, 15, 20, and 50 hidden-layer neurons for each design example. These NN models are denoted by FFBP5, FFBP10, FFBP15, FFBP20, and FFBP50, respectively.

5. NUMERICAL EXAMPLES

The dead load of 2500 kg/m and and live load of 1000 kg/m are applied to all beams. The modulus of elasticity and yield stress of materials are E = 210 GPa and F_y = 235 MPa, respectively. The constitutive law is bilinear with a pure strain hardening slope of 3% of the elastic modulus. The sections of beams and columns are selected from the W-shaped sections listed in Table 1.

Table 1: Available W-shaped sections

Columns				Beams			
No.	Profile	No.	Profile	No.	Profile	No.	Profile
1	W14×48	13	W14×257	1	W12×19	13	W21×50
2	W14×53	14	W14×283	2	W12×22	14	W21×57
3	W14×68	15	W14×311	3	W12×35	15	W24×55
4	W14×74	16	W14×342	4	W12×50	16	W21×68
5	W14×82	17	W14×370	5	W18×35	17	W24×62
6	W14×132	18	W14×398	6	W16×45	18	W24×76
7	W14×145	19	W14×426	7	W18×40	19	W24×84
8	W14×159	20	W14×455	8	W16×50	20	W27×94
9	W14×176	21	W14×500	9	W18×46	21	W27×102
10	W14×193	22	W14×550	10	W16×57	22	W27×114
11	W14×211	23	W14×605	11	W18×50	23	W30×108
12	W14×233	24	W14×665	12	W21×44	24	W30×116

5.1 Five-story SMF

To train and test the NN models, a data set including 400 samples is randomly generated. The components of output vector are shown in Figs. 7 to 9.
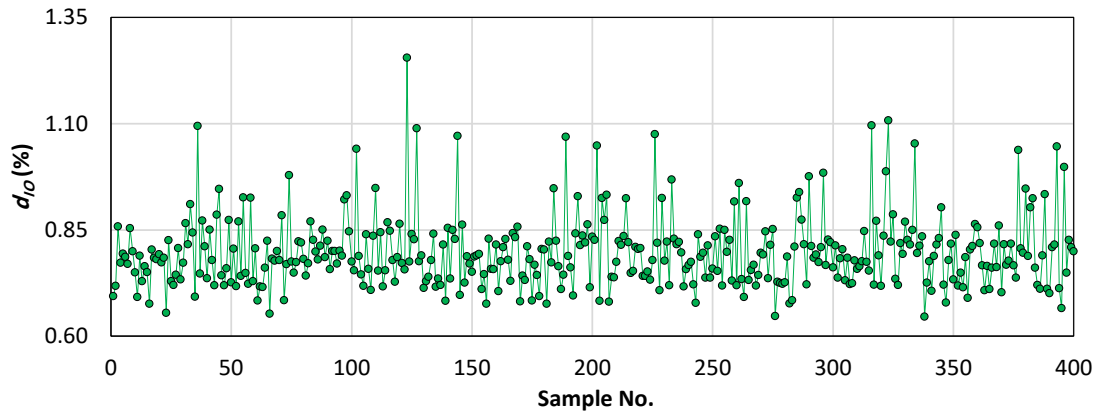
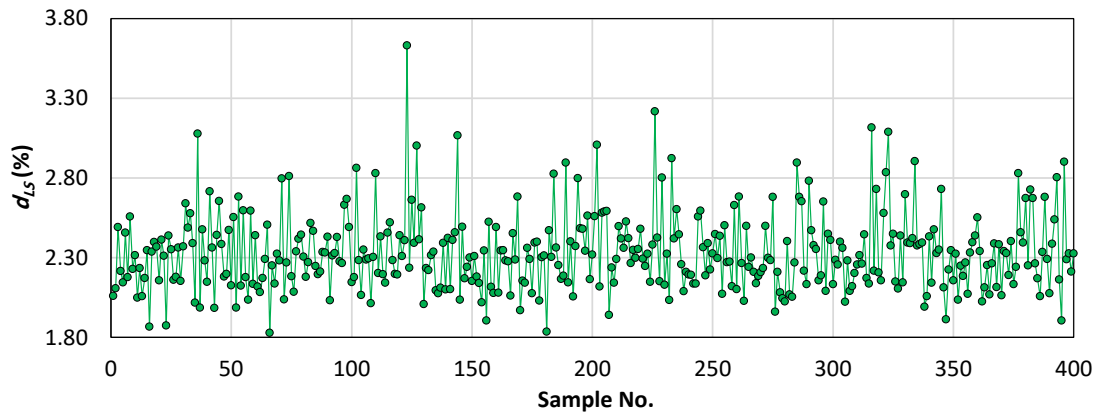Figure 7. Maximum inter-story drift ratios at IO level for 5-story steel MRF

Figure 8. Maximum inter-story drift ratios at LS level for 5-story steel MRF
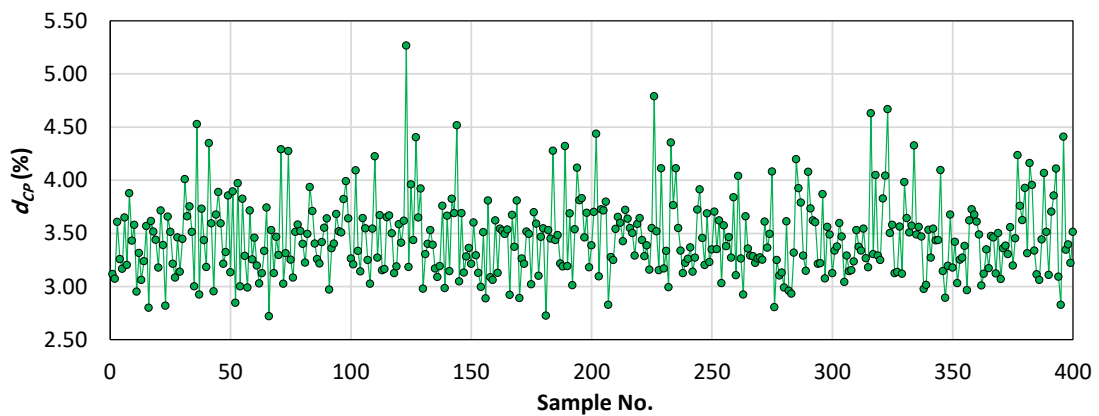
Figure 9. Maximum inter-story drift ratios at CP level for 5-story steel MRF

The FFBP5, FFBP10, FFBP15, FFBP20, and FFBP50 NN models are trained and tested and the results are reported in Tables 2 to 6, in terms of *MAPE*, *RMSE* and R^2.

Table 2: Performance evaluation of FFBP5 for 5-story steel MRF

Phase	Metric	Maximum inter-story drift ratio (%)		
		d_{IO}	d_{LS}	d_{CP}
Training	*MAPE*	3.4205	2.4947	2.5190
	RMSE	0.0342	0.0743	0.1097
	R^2	0.8426	0.9085	0.9136
Testing	*MAPE*	4.4284	3.8692	3.9789
	RMSE	0.0459	0.1147	0.1813
	R^2	0.6266	0.7163	0.7052

Table 3: Performance evaluation of FFBP10 for 5-story steel MRF

Phase	Metric	Maximum inter-story drift ratio (%)		
		d_{IO}	d_{LS}	d_{CP}
Training	*MAPE*	3.1527	1.7704	1.5688
	RMSE	0.0316	0.0513	0.0666
	R^2	0.8658	0.9563	0.9681
Testing	*MAPE*	3.3533	2.8420	2.8230
	RMSE	0.0325	0.0797	0.1200
	R^2	0.8124	0.8631	0.8708

Table 4: Performance evaluation of FFBP15 for 5-story steel MRF

Phase	Metric	Maximum inter-story drift ratio (%)		
		d_{IO}	d_{LS}	d_{CP}
Training	*MAPE*	2.9308	1.3359	1.0111
	RMSE	0.0291	0.0390	0.0435
	R^2	0.8861	0.9748	0.9863
Testing	*MAPE*	3.5865	3.3212	3.6524
	RMSE	0.0358	0.0977	0.1612
	R^2	0.7721	0.7944	0.7672

Table 5: Performance evaluation of FFBP20 for 5-story steel MRF

Phase	Metric	Maximum inter-story drift ratio (%)		
		d_{IO}	d_{LS}	d_{CP}
Training	*MAPE*	2.7863	1.0404	0.6043
	RMSE	0.0277	0.0307	0.0257
	R^2	0.8965	0.9843	0.9952
Testing	*MAPE*	3.7745	4.3199	4.6736
	RMSE	0.0395	0.1273	0.2028
	R^2	0.7225	0.6509	0.6315

Table 6: Performance evaluation of FFBP50 for 5-story steel MRF

| Phase | Metric | Maximum inter-story drift ratio (%) | | |
		d_{IO}	d_{LS}	d_{CP}
Training	$MAPE$	1.0221	0.2032	0.0928
	$RMSE$	0.0106	0.0060	0.0042
	R^2	0.9848	0.9993	0.9998
Testing	$MAPE$	5.6251	5.9895	5.9659
	$RMSE$	0.0568	0.1729	0.2381
	R^2	0.4270	0.3558	0.4921

Figs. 10 to 12 show *AMAPE*, *ARMSE*, and *AR*^{2} for the predicted inter-story drift ratios at IO, LS, and CP performance levels, respectively.
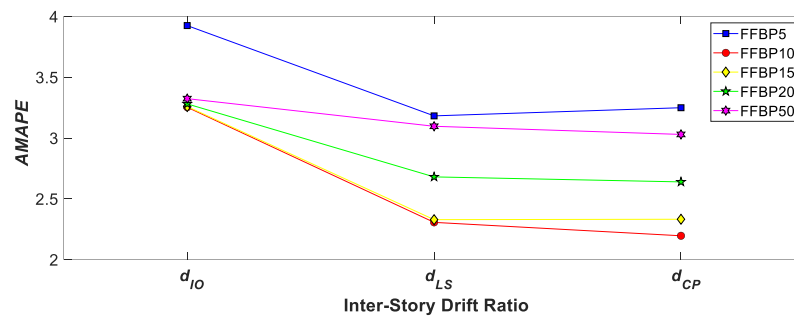
Figure 10. AMAPE of inter-story drift ratios predicted by NN models for 5-story steel SMF
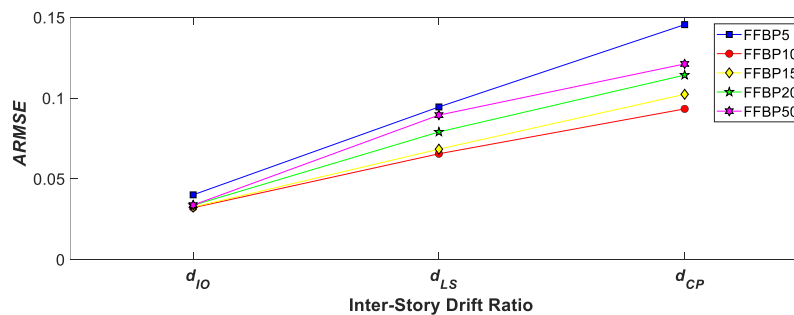
Figure 11. *ARMS*E of inter-story drift ratios predicted by NN models for 5-story steel SMF
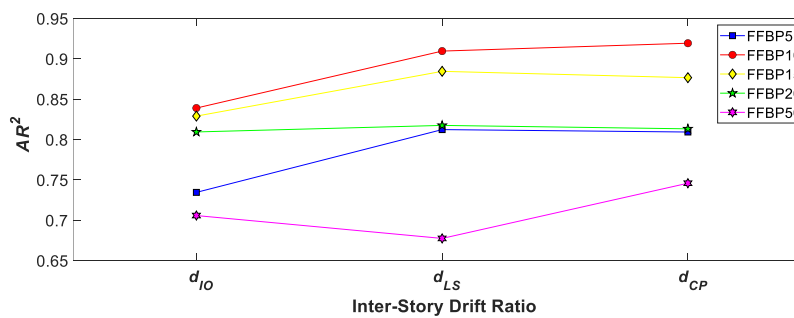
Figure 12. *AR*^{2} of inter-story drift ratios predicted by NN models for 5-story steel SMF

The results show that:
- For d_{IO}, the *AMAPE* of the FFBP10 model is 17.11%, 0.17%, 0.84% and, 2.12% less than the FFBP5, FFBP15, FFBP20 and, FFBP50 NN models, respectively.
- For d_{LS}, the *AMAPE* of the FFBP10 model is 27.52%, 0.96%, 13.95% and, 25.52% less than the FFBP5, FFBP15, FFBP20 and, FFBP50 NN models, respectively.
- For d_{CP}, the *AMAPE* of the FFBP10 model is 32.41%, 5.83%, 16.79% and, 27.51% less than the FFBP5, FFBP15, FFBP20 and, FFBP50 NN models, respectively.
- For d_{IO}, the *ARMSE* of the FFBP10 model is 19.97%, 1.23%, 4.61% and, 4.89% less than the FFBP5, FFBP15, FFBP20 and, FFBP50 NN models, respectively.
- For d_{LS}, the *ARMSE* of the FFBP10 model is 30.69%, 4.17%, 17.09% and, 26.77% less than the FFBP5, FFBP15, FFBP20 and, FFBP50 NN models, respectively.
- For d_{CP}, the *ARMSE* of the FFBP10 model is 35.88%, 8.84%, 18.34% and, 22.99% less than the FFBP5, FFBP15, FFBP20 and, FFBP50 NN models, respectively.
- For d_{IO}, the AR^2 of the FFBP10 model is 14.22%, 1.21%, 3.66% and, 18.87% greater than the FFBP5, FFBP15, FFBP20 and, FFBP50 NN models, respectively.
- For d_{LS}, the AR^2 of the FFBP10 model is 11.98%, 2.84%, 11.26% and, 34.26% less than the FFBP5, FFBP15, FFBP20 and, FFBP50 NN models, respectively.
- For d_{CP}, the AR^2 of the FFBP10 model is 13.59%, 4.87%, 13.04% and, 23.26% less than the FFBP5, FFBP15, FFBP20 and, FFBP50 NN models, respectively.

The numerical results demonstrate that the FFBP NN model with 10 hidden layer neurons outperforms the other models in predicting the inter-story drift ratios at IO, LS, and CP seismic performance levels.

Figs. 13 and 14 display the Absolute Percentage Error (APE) of the predicted maximum inter-story drifts, along with the regression results during the training and testing phases for the NN model with the best prediction accuracy.
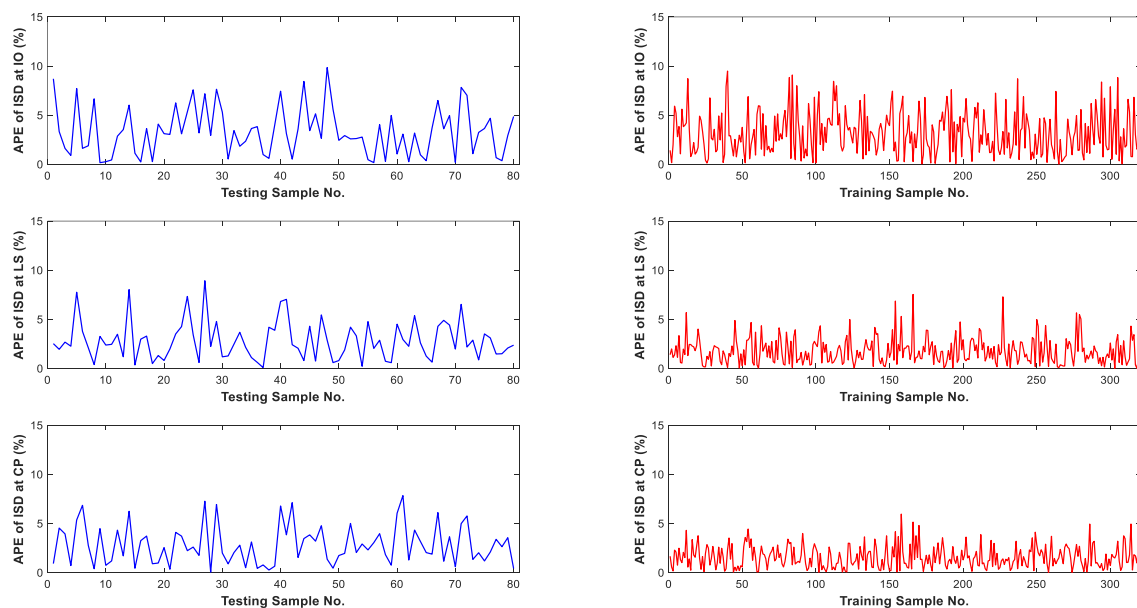

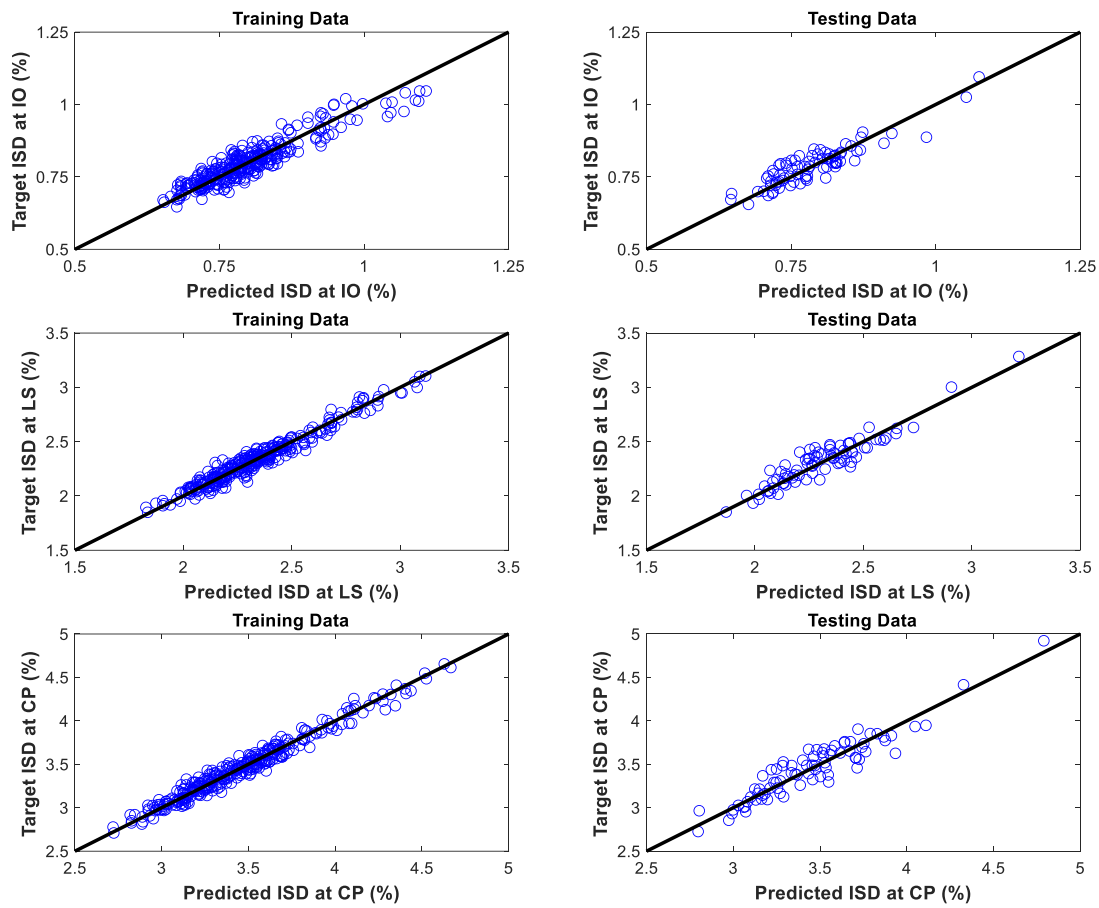Figure 13. APEs of the predicted inter-story drifts using 10 neurons for 5-story steel MRF

Figure 14. Prediction of inter-story drifts using 10 neurons for 5-story steel MRF

5.2 Ten-story SMF

A data set including 600 samples is randomly generated to train and test the NN models. The components of the output vector are shown in Figs. 15 to 17.
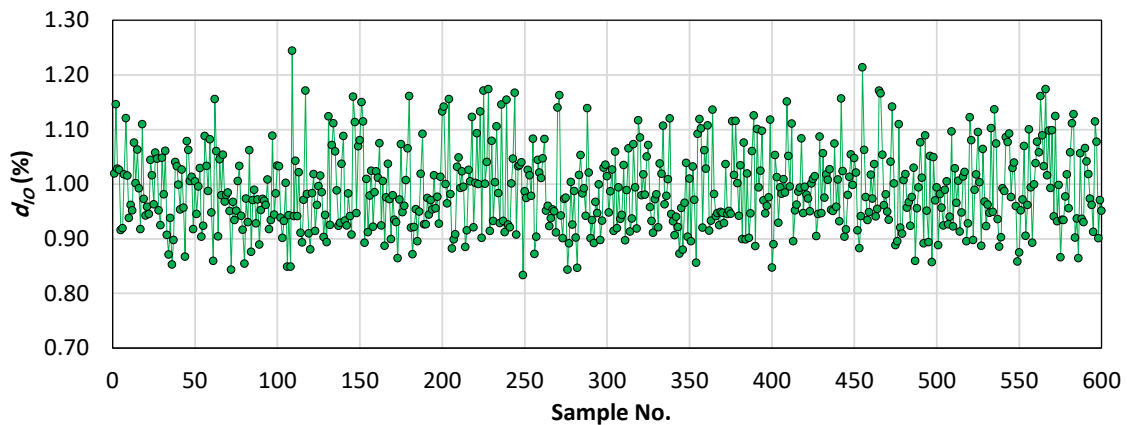

Figure 15. Maximum inter-story drift ratios at IO level for 10-story steel MRF
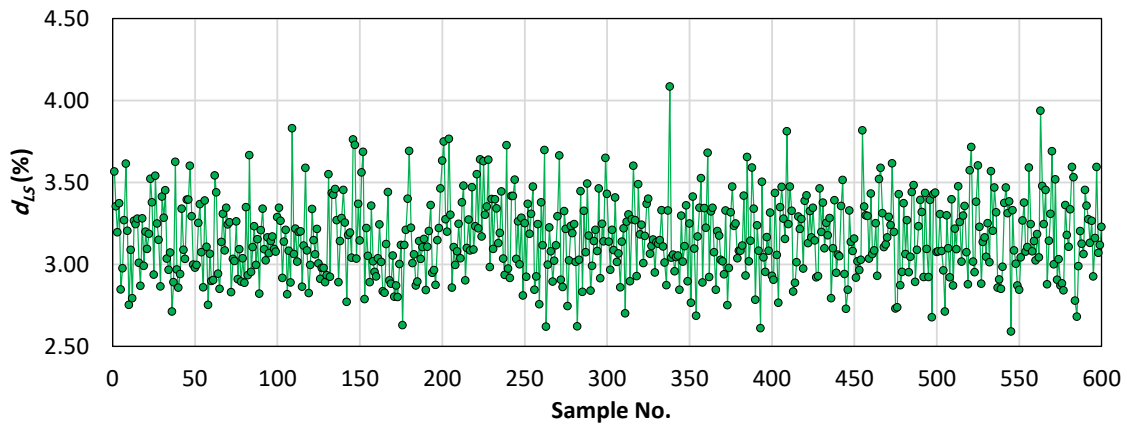
Figure 16. Maximum inter-story drift ratios at LS level for 10-story steel MRF
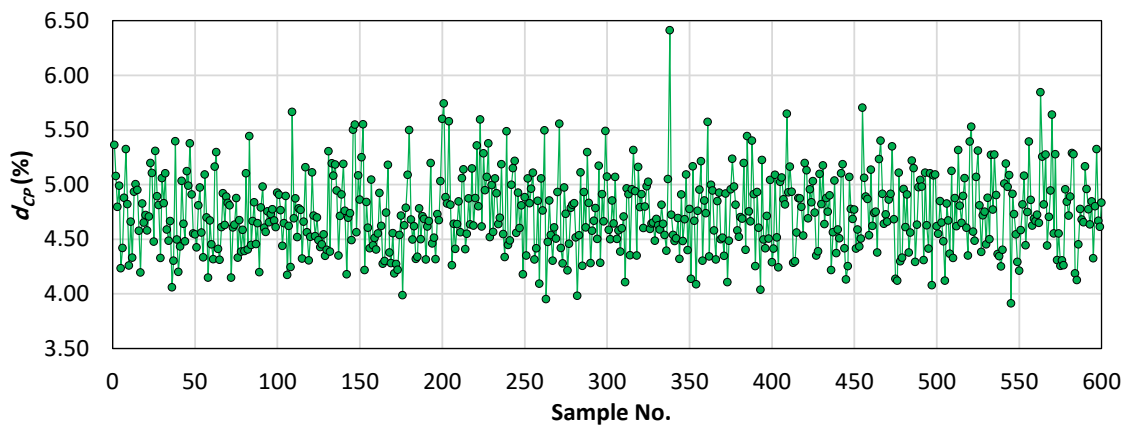

Figure 17. Maximum inter-story drift ratios at CP level for 10-story steel MRF

The FFBP5, FFBP10, FFBP15, FFBP20, and FFBP50 NN models are trained and tested to predict the inter-story drift ratios at IO, LS, and CP seismic performance levels for the 12-story steel frame. The obtained results are reported in Tables 7 to 11 in terms of *MAPE*, *RMSE,* and R^2.

Table 7: Performance evaluation of FFBP5 for 10-story steel MRF

Phase	Metric	Maximum inter-story drift ratio (%)		
		d_{IO}	d_{LS}	d_{CP}
Training	*MAPE*	3.3977	1.5321	1.3050
	RMSE	0.0428	0.0593	0.0773
	R^2	0.6657	0.9412	0.9535
Testing	*MAPE*	4.0157	2.3134	2.1223
	RMSE	0.0501	0.0930	0.1244
	R^2	0.5700	0.8316	0.8567

Table 8: Performance evaluation of FFBP10 for 10-story steel MRF

Phase	Metric	Maximum inter-story drift ratio (%)		
		d_{IO}	d_{LS}	d_{CP}
Training	MAPE	2.9572	0.9708	0.6961
	RMSE	0.0364	0.0378	0.0415
	R^2	0.7590	0.9762	0.9866
Testing	MAPE	3.4241	2.3648	2.1793
	RMSE	0.0424	0.0946	0.1317
	R^2	0.6919	0.8256	0.8393

Table 9: Performance evaluation of FFBP15 for 10-story steel MRF

Phase	Metric	Maximum inter-story drift ratio (%)		
		d_{IO}	d_{LS}	d_{CP}
Training	MAPE	2.8523	0.6894	0.3819
	RMSE	0.0350	0.0273	0.0231
	R^2	0.7769	0.9874	0.9958
Testing	MAPE	3.8279	3.2561	2.9862
	RMSE	0.0472	0.1265	0.1778
	R^2	0.6185	0.6882	0.7071

Table 10: Performance evaluation of FFBP20 for 10-story steel MRF

Phase	Metric	Maximum inter-story drift ratio (%)		
		d_{IO}	d_{LS}	d_{CP}
Training	MAPE	2.2760	0.6107	0.2892
	RMSE	0.0275	0.0239	0.0173
	R^2	0.8622	0.9904	0.9976
Testing	MAPE	3.9181	3.7783	3.7052
	RMSE	0.0478	0.1497	0.2172
	R^2	0.6087	0.5635	0.5629

Table 11: Performance evaluation of FFBP50 for 10-story steel MRF

Phase	Metric	Maximum inter-story drift ratio (%)		
		d_{IO}	d_{LS}	d_{CP}
Training	MAPE	6.48e-06	1.23e-06	1.13e-06
	RMSE	8.01e-08	4.78e-08	6.47e-08
	R^2	1	1	1
Testing	MAPE	5.6618	4.0869	3.7060
	RMSE	0.0741	0.1714	0.2278
	R^2	0.0595	0.4278	0.5194

Figs. 18 to 20 show *AMAPE*, *ARMSE*, and *AR*^{2} for the predicted inter-story drift ratios at IO, LS, and CP performance levels, respectively.
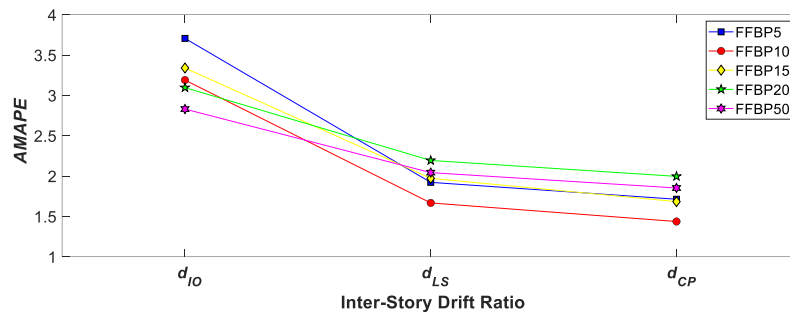
Figure 18. AMAPE of inter-story drift ratios predicted by NN models for 10-story steel SMF
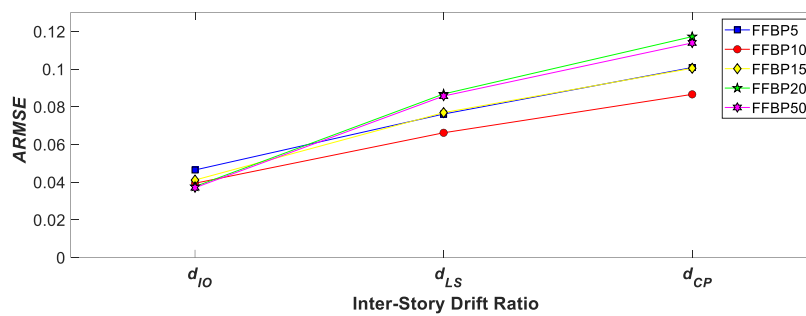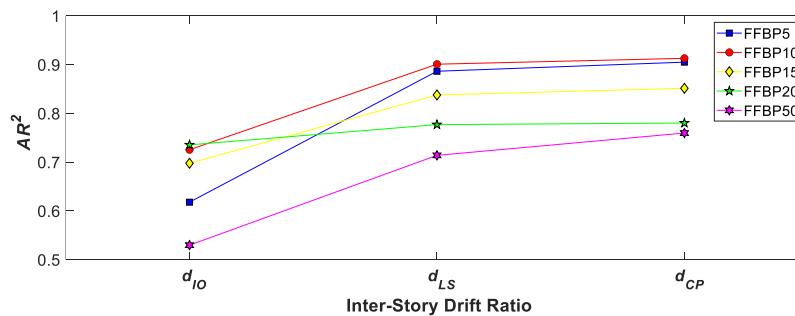

Figure 19. *ARMS*E of inter-story drift ratios predicted by NN models for 10-story steel SMF

Figure 20. AR^2 of inter-story drift ratios predicted by NN models for 10-story steel SMF

The results show that:
- For d_{IO}, the *AMAPE* of the FFBP20 and FFBP50 NN models is 2.93% and 11.28% less than the FFBP10 model. The *AMAPE* of FFBP10 is 13.92% and 4.47% less than the FFBP5 and FFBP15 models, respectively.
- For d_{LS}, the *AMAPE* of the FFBP10 model is 13.26%, 15.46%, 24.00% and, 18.38% less than the FFBP5, FFBP15, FFBP20 and, FFBP50 NN models, respectively.
- For d_{CP}, the *AMAPE* of the FFBP10 model is 16.10%, 14.63%, 28.01% and 22.41% less than the FFBP5, FFBP15, FFBP20 and FFBP50 NN models, respectively.
- For d_{IO}, the *ARMS*E of the FFBP10 model is 15.18% and 4.14% less than the FFBP5 and FFBP15 and 4.65% and 6.34% greater than the FFBP20 and FFBP50 models, respectively.
- For d_{LS}, the *ARMSE* of the FFBP10 model is 13.07%, 13.91%, 23.73% and, 22.75% less than the FFBP5, FFBP15, FFBP20 and, FFBP50 NN models, respectively.
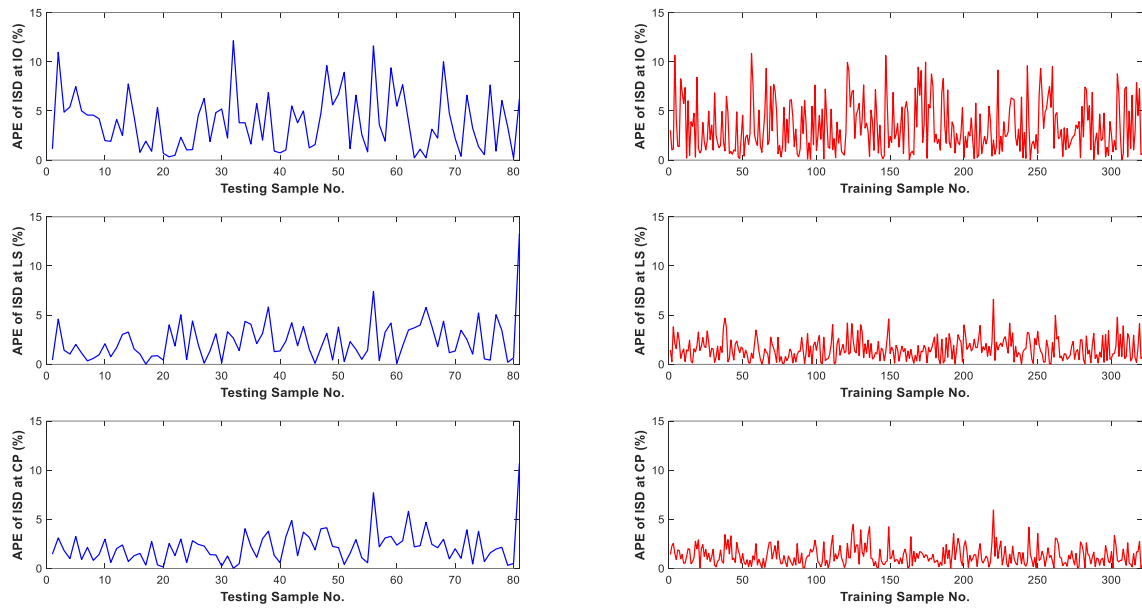
Figure 21. APEs of the predicted inter-story drifts using 10 neurons for 5-story steel MRF
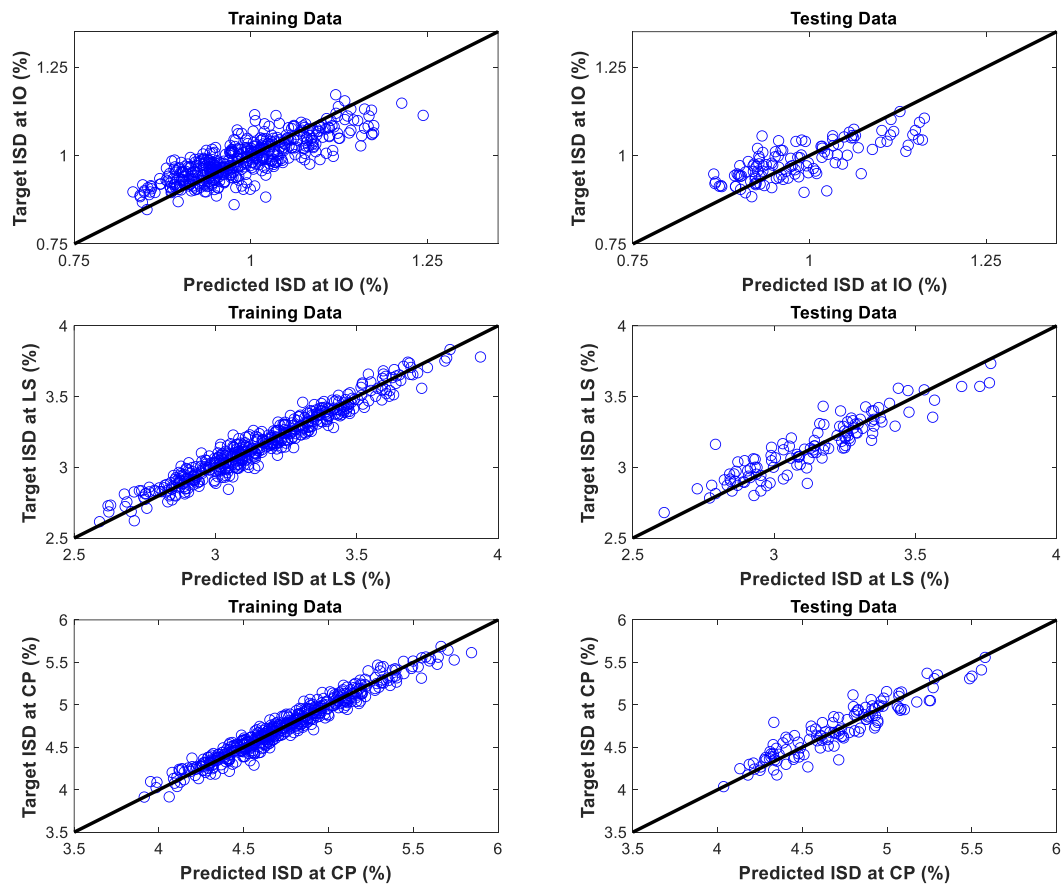

Figure 22. Prediction of inter-story drifts using 10 neurons for 5-story steel MRF

- For d_{CP}, the *ARMSE* of the FFBP10 model is 14.13%, 13.79%, 26.14% and, 23.97% less than the FFBP5, FFBP15, FFBP20 and, FFBP50 NN models, respectively.
- For d_{IO}, the AR^2 of the FFBP10 model is 17.41%, 3.98% and, 36.94% greater than the FFBP5, FFBP15 and FFBP50 NN models, respectively. In addition, the AR^2 of the FFBP10 model is 1.36%, less than the FFBP20 NN model.
- For d_{LS}, the AR^2 of the FFBP10 model is 1.64%, 7.53%, 15.95% and, 26.19% less than the FFBP5, FFBP15, FFBP20 and, FFBP50 NN models, respectively.
- For d_{CP}, the AR^2 of the FFBP10 model is 0.87%, 7.22%, 17.00% and, 20.17% less than the FFBP5, FFBP15, FFBP20 and FFBP50 NN models, respectively.

The numerical results demonstrate that the FFBP NN model with 10 hidden layer neurons outperforms the other models in predicting the inter-story drift ratios at IO, LS, and CP seismic performance levels.

Figs. 21 and 22 display the APE of the predicted maximum inter-story drifts, along with the regression results during the training and testing phases for the NN model with the best prediction accuracy for 10-story steel MRF.

6. CONCLUSIONS

The primary goal of this paper is to develop a neural network-based approach for assessing the seismic responses of steel moment-resisting frames. The maximum inter-story drift ratios at IO, LS, and CP seismic performance levels are considered the desired seismic responses of the frames. This involves using a feedforward-backpropagation neural network instead of pushover static nonlinear analysis. Two numerical examples of 5- and 10-story steel MRFs are illustrated, and datasets containing 400 and 600 samples are randomly generated for them, respectively. Five feedforward-backpropagation neural network models with 5, 10, 15, 20, and 50 hidden-layer neurons are considered for each illustrative example. Notably, the model with 10 hidden layer neurons consistently outperforms the other models in accurately predicting inter-story drift ratios at different performance levels, as confirmed by the numerical results of both examples.

REFERENCES

1. FEMA-356, *Prestandard and Commentary for the Seismic Rehabilitation of Buildings*. Federal Emergency Management Agency, Washington DC, 2000.
2. Kaveh A, Zakian P. Performance based optimal seismic design of RC shear walls incorporating soil–structure interaction using CSS algorithm. *Int J Optim Civil Eng* 2012; **2**: 383–405.
3. Liang JC, Li LJ, He JN. Performance-based multi-objective optimum design for steel structures with intelligence algorithms. *Int J Optim Civil Eng* 2015; **5**: 79–101.
4. Gholizadeh S. Performance-based optimum seismic design of steel structures by a modified firefly algorithm and a new neural network. *Adv Eng Softw* 2015; **81**: 50–65.

5. Rahami H, Mohebian P, Mousavi M. Performance-based connection topology optimization of unbraced and X-braced steel frames. *Int J Optim Civil Eng* 2017; **7**:451–68.

6. Ganjavi B, Hajirasouliha I. Optimum performance-based design of concentrically braced steel frames subjected to near-fault ground motion excitations. *Int J Optim Civil Eng* 2019; **9**:177–193.

7. Gholizadeh S, Ebadijalal M. Performance based discrete topology optimization of steel braced frames by a new metaheuristic. *Adv Eng Softw* 2018; **123**: 77–92.

8. Kaveh A, Zolghadr A. Topology optimization of trusses considering static and dynamic constraints using the CSS. *Appl Soft Comput*, 2013; **13**: 2727–34.

9. Kaveh A, Javadi SM. Shape and size optimization of trusses with multiple frequency constraints using harmony search and ray optimizer for enhancing the particle swarm optimization algorithm. *Acta Mech*, 2014; **225**: 1595–606.

10. Kaveh A, Mirzaei B, Jafarvand A. An improved magnetic charged system search for optimization of truss structures with continuous and discrete variables. *Appl Soft Comput*, 2015; **28**: 400–10.

11. Kaveh A, Talatahari S. An enhanced charged system search for configuration optimization using the concept of fields of forces. *Struct Multidiscip Optim*, 2011; **43**: 339–51.

12. Kaveh A, Talatahari S. A charged system search with a fly to boundary method for discrete optimum design of truss structures. *Asian J Civil Eng*, 2010; **11**: 277–293.

13. Kaveh A, Bakhshpoori T, Hamze-Ziabari SM. GMDH-based prediction of shear strength of FRP-RC beams with and without stirrups. *Comput Concr* 2018;**22**:197–207.

14. Kaveh A, Eskandari A. Analysis of double-layer barrel vaults using different neural networks; a comparative study. *Int J Optim Civil Eng* 2021;**11**:113-141.

15. Kaveh A, Dadras Eslamlou A, Javadi SM, Geran Malek N. Machine learning regression approaches for predicting the ultimate buckling load of variable-stiffness composite cylinders. Acta Mechanica 2021;**232**:921-31.

16. Kaveh A, Khavaninzadeh N. Efficient training of two ANNs using four meta-heuristic algorithms for predicting the FRP strength. *Structures* 2023;**52**:256–72.

17. Kaveh A, Seddighian MR, Farsi N. A metaheuristic-based artificial neural network for plastic limit analysis of frames. *Int J Optim Civil Eng* 2023;**13**:143-54.

18. Standard No. 2800. Iranian Code of Practice for Seismic Resistant Design of Buildings, Building and Housing Research Center, Tehran, 2014.

19. *OpenSees*. Open System For Earthquake Engineering Simulation. ver 3.3.0 [Computer software]. PEER, Berkeley, CA.

20. Fattahi F, Gholizadeh S. Seismic fragility assessment of optimally designed steel moment frames. *Eng Struct* 2019;**179**:37–51.

21. Gholizadeh S, Danesh M, Gheyratmand C. A new Newton metaheuristic algorithm for discrete performance-based design optimization of steel moment frames. *Comput Struct* 2020;**234**:106250.

22. Ghaderi M, Gholizadeh S. Mainshock–aftershock low-cycle fatigue damage evaluation of performance-based optimally designed steel moment frames. *Eng Struct* 2021;**237**:112207.

23. Gholizadeh S, Hasançebi O, Eser H, Koçkaya O. Seismic collapse safety based optimization of steel Moment-Resisting frames. *Structures* 2022;**237**:112207.
24. Hagan MT, Demuth HB, Beal MH. Neural network design, PWS Publishing Company, Boston, 1996.
25. AISC 360-16. Specification for structural steel buildings. Chicago: American Institute of Steel Construction; 2016.